Computers in Biology and Medicine 105 (2019) 72–80

Contents lists available at ScienceDirect

Computers in Biology and Medicine

journal homepage: www.elsevier.com/locate/compbiomed

Automated glaucoma diagnosis using bit-plane slicing and local binary pattern techniques

Shishir Maheshwari[a,*], Vivek Kanhangad[a], Ram Bilas Pachori[a], Sulatha V. Bhandary[b], U. Rajendra Acharya[c,d,e]

[a] *Discipline of Electrical Engineering, Indian Institute of Technology Indore, Indore, 453552, India*
[b] *Department of Ophthalmology, Kasturba Medical College, Manipal, 576104, India*
[c] *Department of Electronics and Communication Engineering, Ngee Ann Polytechnic, 599489, Singapore*
[d] *Department of Biomedical Engineering, School of Science and Technology, SUSS University, 599491, Singapore*
[e] *School of Medicine, Faculty of Health and Medical Sciences, Taylor's University, 47500, Subang Jaya, Malaysia*

ARTICLE INFO

Keywords:
Glaucoma
Bit-plane slicing
Local binary pattern
Support vector machine
Decision level fusion

ABSTRACT

Background and objective: Glaucoma is a ocular disorder which causes irreversible damage to the retinal nerve fibers. The diagnosis of glaucoma is important as it may help to slow down the progression. The available clinical methods and imaging techniques are manual and require skilled supervision. For the purpose of mass screening, an automated system is needed for glaucoma diagnosis which is fast, accurate, and helps in reducing the burden on experts.

Methods: In this work, we present a bit-plane slicing (BPS) and local binary pattern (LBP) based novel approach for glaucoma diagnosis. Firstly, our approach separates the red (R), green (G), and blue (B) channels from the input color fundus image and splits the channels into bit planes. Secondly, we extract LBP based statistical features from each of the bit planes of the individual channels. Thirdly, these features from the individual channels are fed separately to three different support vector machines (SVMs) for classification. Finally, the decisions from the individual SVMs are fused at the decision level to classify the input fundus image into normal or glaucoma class.

Results: Our experimental results suggest that the proposed approach is effective in discriminating normal and glaucoma cases with an accuracy of 99.30% using 10-fold cross validation.

Conclusions: The developed system is ready to be tested on large and diverse databases and can assist the ophthalmologists in their daily screening to confirm their diagnosis, thereby increasing accuracy of diagnosis.

1. Introduction

Glaucoma is a ocular disorder which may lead to permanent blindness. According to world health organization (WHO), glaucoma is considered as the second leading cause of vision loss after cataract [1]. Due to blockage in the outflow of aqueous humor, the intra-ocular pressure (IOP) within the eye increases. This increase in pressure damages the optic nerves causes visual field defects. The damage in optic nerves is irreversible and cannot be cured [2]. Also, the symptoms are untraceable in the initial stage which later become incurable due to unspecific rate of progression. However, early diagnosis may help to slow down the progression of glaucoma [3].

There are two types of glaucoma based on drainage network blockage [4]: open angle glaucoma and closed angle glaucoma. Former is commonly found and is characterized by its slow progression. However, the there are no obvious symptoms and the affected person will know only at a late stage. This condition affects the visual field not the central vision in the early stage. Angle closure glaucoma usually presents with eye pain, redness and decreased vision.This occurs due to rapid obstruction of the aqueous outflow. This condition receives immediate attention and thus immediate treatment.

Ophthalmologists advise regular eye checkups to prevent glaucoma progression for patients. The following clinical instruments are commonly used to diagnose glaucoma [5]:

- tonometer is used to measure IOP within eye.
- ophthalmoscope is used to examine retinal structures such as nerve fibers, and optic disk for glaucoma damage.

---

[*] Corresponding author.
E-mail address: phd1501102003@iiti.ac.in (S. Maheshwari).

https://doi.org/10.1016/j.compbiomed.2018.11.028
Received 5 October 2018; Received in revised form 30 November 2018; Accepted 30 November 2018

- perimetry is used to test patient's visual field.
- gonioscope is used to evaluate the internal drainage system.
- pachymeter is used to measure cornea thickness.

Aforementioned clinical techniques are manual, time consuming, and require skilled supervision. In addition, the retinal imaging devices such as confocal scanning laser ophthalmoscope (CSLO), scanning laser polarimeter (SLP), and optical coherence tomograph (OCT) generate retinal images, which provide information about nerve fibers and optic disk. These tests need pupillary dilatation and are costly. They are used for confirming the diagnosis and not for screening. The results may vary depending upon intra/inter observer [1]. Hence for mass screening, we need to have an automated glaucoma diagnosis system that is fast, accurate, and can help in reducing the burden on the experts.

As opposed to these bulkier retinal imaging devices, fundus cameras are generally portable and economical [6]. The acquired fundus images can be used to visualize optic disc, retina and blood vessels. The analysis of fundus images has been performed to detect other ocular disorders including diabetic retinopathy [7], and macula degeneration [9]. Glaucoma can be characterized by structural changes such as cup-to-disc ratio (CDR), cup diameter and, loss in nerve fibers [8].

Of late, various computational algorithms have been proposed for fundus image-based glaucoma diagnosis. Authors in Refs. [10,11] employed CDR value for glaucoma diagnosis. Specifically, the authors in Ref. [10] have employed contour based segmentation approach for CDR computation. The authors in Ref. [11] have proposed depth discontinuity based methodology which employed cup boundary for estimating CDR. Fleming et al. [12] have proposed Hough transform based approach for computing CDR. Apart from the CDR based approaches, many signal decomposition approaches have been developed for computer aided diagnosis (CAD) of glaucoma. The authors in Ref. [2] have developed a higher order spectra based methodology for glaucoma diagnosis. Dua et al. [3] used discrete wavelet transform (DWT) based energy features followed by supervised classification process. Empirical wavelet transform (EWT) and least squares suppport vector machine (LS-SVM) based glaucoma diagnosis approach have been developed in Ref. [13]. In another work [8], the same authors have employed iterative variational mode decomposition (VMD) on a larger glaucoma dataset. Authors in Ref. [1] have proposed a methodology using texton and local configuration patterns. Recently, an eighteen layer deep convolutional neural network (CNN) has been proposed for glaucoma diagnosis [5]. A summary of the existing glaucoma diagnosis methodologies is presented in Table 5.

The rest of this paper is structured as follows. Section II provides a detailed description of the proposed methodology, along with feature normalization and ranking, and classification. The description of the database, followed by experimental results is presented in Section III. Discussion is presented in Section IV. Finally, the paper is concluded with a note on future work in Section V.

2. Method

This section presents a methodology for glaucoma diagnosis. A few sample images are shown in Fig. 1. The block diagram of the proposed methodology is illustrated in Fig. 2. The proposed methodology starts with a preprocessing step, in which the input fundus image is resized to 360×480 pixels to decrease the computation time. The resized RGB image is then separated into red (R), green (G), and blue (B) channels. Each of these channels undergo contrast limited adaptive histogram equalization (CLAHE) [14,15] to overcome the problem of uneven lighting conditions at the time of fundus image acquisition.

Bit-plane slicing (BPS) splits each of the preprocessed channels into bit planes. Local binary patterns (LBP) generates LBP images from bit planes. Further, the statistical features are extracted from LBP images and extracted features are subjected to normalization and ranking. The ranked features are further fed to support vector machine (SVM) classifier and decision level based fusion is performed to discriminate the two classes automatically.

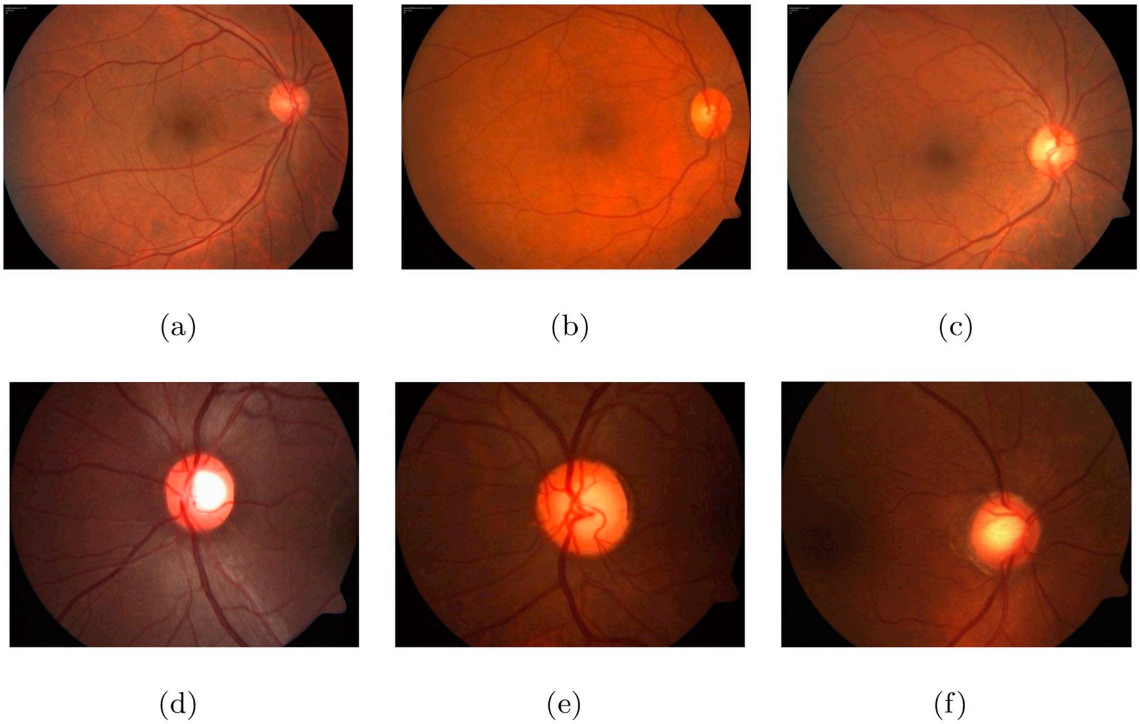

Fig. 1. Sample fundus images: normal (top row) and glaucoma (bottom row) class.

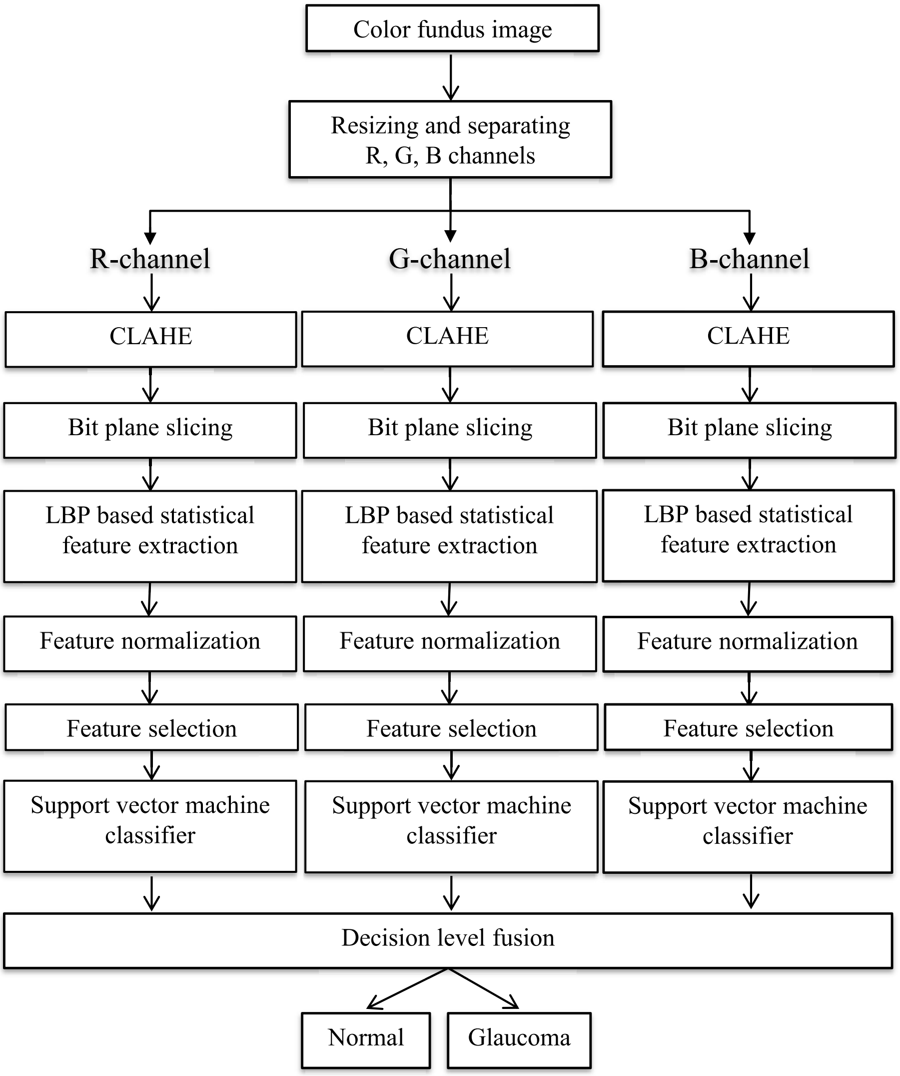

Fig. 2. Block diagram of the proposed methodology.

2.1. *Bit plane slicing*

Bit plane slicing (BPS) [14] is a technique which splits a gray image into its bit planes. In general, a 256-level gray scale image is composed of 8-bits and therefore BPS splits it into 8 bit planes. In this work, we have R, G, and B channels and each channel is a 256-level gray scale image. Therefore, there are 8 bit planes for each channel. BPS is useful for analyzing the relative importance of each bit plane, which can be processed further to extract the discriminating information. First and third rows of Fig. 3 show bit planes of R channel of glaucoma image (shown in Fig. 1(e)). Fig. 3(a) shows the least significant bit (LSB) plane. Similarly, Fig. 3(b) – 3(d) and Fig. 3(i) – 3(l) show the remaining bit planes.

2.2. *Local binary patterns based feature extraction*

The analysis of two-dimensional texture has been investigated extensively for applications involving image classification. In real world, textures are often irregular due to orientation, scale, lighting conditions [16]. Most of the discriminating problems rely heavily on how effectively the variations in texture is encoded.

The LBP [16] is a simple and effective image texture descriptor that has been widely used for diverse applications. In order to capture the local changes in each of the bit planes, we employ local binary pattern (LBP) based features. LBP is computed by performing logical operations in local neighborhood of a predefined window. More specifically, the computation of LBP involves two steps. In first step, each of the neighboring pixels is thresholded against the center pixel value to generate a binary pattern. In second step, the binary pattern is converted into its equivalent decimal value. This decimal value is considered the LBP of the corresponding center pixel.

Since the bit planes are binary in nature, we have directly performed the second step to compute the LBP. Mathematically, it is computed as follows:

$$\mathrm{LBP}_{N,L} = \sum_{n=0}^{N-1} x_n * 2^n \tag{1}$$

where x_n is the binary value of the neighboring pixels. N and L in Eq. (1) are the number of local neighbors and the size of the square window, respectively. In our experiments, the values of N and L are set to 8 and 3, respectively. In this work, we have extracted LBPs from each of the

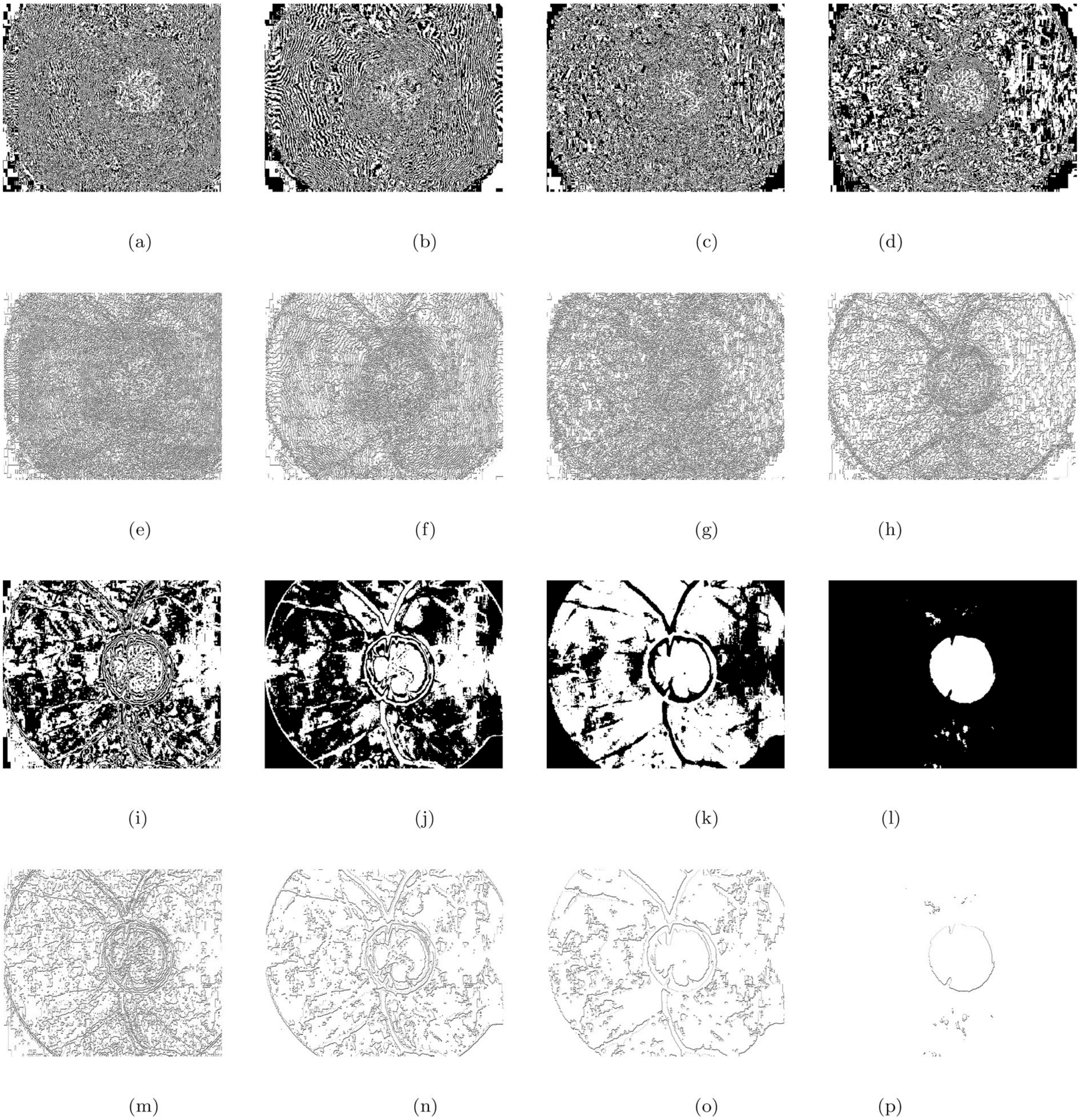

Fig. 3. 1st & 3rd row: Bit planes; 2nd & row: LBP images of R channel of the glaucoma image in Fig. 1(e).

bit planes. Hence, this process generates a 2D LBP array or a LBP image from each of the bit planes. Second and fourth rows of Fig. 3 show the LBP images corresponding to the bit planes shown in Fig. 3(a)-3(d) and Fig. 3(i)-3(l).

LBP is an efficient descriptor that characterizes local variation in gray levels, which is useful for texture based classification problems. The LBP images computed from bit planes incorporate local bit level changes. More often, the statistical analysis of texture has been found to be effective in capturing the underlying discriminating information present in the form of randomness and variability. Specifically, we compute non-Shannon entropies and fractal dimension from LBP image as statistical features. These features are further detailed below.

2.2.1. *Entropy*

Entropy measures the variation in texture as an information content [17]. Uniform distribution of pixel values leads to zero information content in an image. We have used non-shannon entropies namely, Kapur entropy (KE) [18], and Renyi entropy (RE) [18] to determine the texture randomness associated with LBP vector. These entropies provide higher dynamic range that makes better estimates of randomness. The mathematical expressions for KE and RE are given below [19]:

$$\mathrm{KE} = \frac{1}{\mathfrak{b} - \mathfrak{a}} \log_2 \left(\frac{\sum_{i=0}^{I-1} p_i^{\mathfrak{a}}}{\sum_{i=0}^{I-1} p_i^{\mathfrak{b}}} \right) \tag{2}$$

$$RE = \frac{1}{1-\alpha}\log_2\left(\sum_{i=0}^{I-1} p_i^{\alpha}\right) \tag{3}$$

where p_i denotes the probability of occurrence of i^{th} LBP value. If a LBP value occurs m number of times, then p_i is computed as:

$$p_i = \frac{m}{r \times c} \tag{4}$$

where r and c denote the number of rows and columns of LBP vector, respectively.

2.2.2. Fractal dimension

Of late, fractal dimension (FD) has been found to be effective in diagnosis of ovarian tumor [20] and epileptic seizures [21]. A fractal is a smallest unit which repeats itself into self similar patterns that manifest at every scale [21]. They are used to analyze random phenomena. FD is a measure of roughness and self-similarity. In this work, we have used the sequential box counting (SBC) [22] method for computing FD.

2.3. Feature normalization

The performance of machine learning algorithms may get affected by skewed data, which can result in false alarm. Normalization of data brings the skewed data to desired numeric scale. In our proposed approach, we have used z-score normalization [23] that normalizes the data into zero mean and unit standard deviation.

2.4. Feature selection

Feature selection helps to improve the performance of the computer aided diagnosis systems. Some of the extracted features do not contribute significantly to the performance due to their low discriminating ability. In this work, we have employed Student's *t*-test [24,25] for feature selection. Student's *t*-test generates *t* value for each of the features. The *t* value denotes the discriminating capability of the corresponding feature. A high *t* value indicates higher discriminating capability. Therefore, these features are arranged in descending order of their corresponding *t* values. Tables 1–3 show the first twenty features and their corresponding *t* values. In Features column, subscript denotes the bit plane number.

Table 1
Features extracted with *t* values for R channel.

Features	Normal	Glaucoma	*t* value
	(*mn* ± *std*)	(*mn* ± *std*)	
RE_4	0.04 ± 0.008	0.02 ± 0.008	49.60
KE_4	0.52 ± 0.033	0.40 ± 0.058	48.45
RE_3	0.06 ± 0.005	0.03 ± 0.011	47.92
KE_5	0.41 ± 0.043	0.28 ± 0.065	43.67
RE_2	0.05 ± 0.006	0.03 ± 0.010	43.06
KE_3	0.57 ± 0.016	0.48 ± 0.059	42.16
RE_5	0.02 ± 0.006	0.008 ± 0.005	40.35
KE_6	0.29 ± 0.046	0.18 ± 0.054	40.09
KE_2	0.55 ± 0.023	0.55 ± 0.062	40.01
FD_5	3.87 ± 0.010	3.84 ± 0.023	37.93
FD_4	3.89 ± 0.005	3.87 ± 0.016	36.57
FD_6	3.83 ± 0.019	3.77 ± 0.037	35.69
KE_7	0.19 ± 0.042	0.12 ± 0.044	35.24
RE_7	0.06 ± 0.004	0.04 ± 0.011	34.11
KE_8	0.15 ± 0.030	0.09 ± 0.033	34.01
RE_6	0.008 ± 0.003	0.003 ± 0.002	33.10
FD_7	3.75 ± 0.03	3.68 ± 0.052	32.33
KE_1	0.58 ± 0.013	0.52 ± 0.046	31.44
FD_3	3.90 ± 0.003	3.88 ± 0.014	29.56
RE_8	0.0017 ± 0.0008	0.0006 ± 0.0005	28.69

mn: mean *std*: standard deviation.

Table 2
Features extracted with *t* values for G channel.

Features	Normal	Glaucoma	*t* value
	(*mn* ± *std*)	(*mn* ± *std*)	
RE_3	0.05 ± 0.006	0.03 ± 0.011	50.89
KE_4	0.52 ± 0.038	0.40 ± 0.056	49.62
RE_4	0.04 ± 0.008	0.02 ± 0.007	49.30
RE_1	0.05 ± 0.007	0.03 ± 0.009	47.14
KE_5	0.42 ± 0.043	0.29 ± 0.064	46.56
KE_6	0.30 ± 0.041	0.18 ± 0.058	45.73
KE_3	0.57 ± 0.019	0.47 ± 0.058	45.21
KE_1	0.56 ± 0.024	0.46 ± 0.053	43.89
RE_5	0.02 ± 0.006	0.008 ± 0.005	43.36
KE_2	0.50 ± 0.038	0.39 ± 0.057	42.73
RE_2	0.04 ± 0.008	0.02 ± 0.007	41.89
RE_6	0.01 ± 0.003	0.003 ± 0.002	40.39
FD_4	3.89 ± 0.006	3.87 ± 0.018	38.43
FD_5	3.87 ± 0.013	3.83 ± 0.029	35.98
FD_6	3.82 ± 0.024	3.75 ± 0.048	35.92
FD_2	3.89 ± 0.006	3.87 ± 0.014	34.07
KE_8	0.16 ± 0.050	0.07 ± 0.048	32.88
FD_3	3.90 ± 0.003	3.88 ± 0.017	32.18
FD_1	3.90 ± 0.003	3.88 ± 0.009	30.96
FD_8	3.55 ± 0.116	3.34 ± 0.127	30.83

mn: mean *std*: standard deviation.

Table 3
Features extracted with *t* values for B channel.

Features	Normal	Glaucoma	*t* value
	(*mn* ± *std*)	(*mn* ± *std*)	
RE_3	0.06 ± 0.006	0.03 ± 0.011	55.14
RE_1	0.05 ± 0.007	0.03 ± 0.010	54.65
KE_1	0.56 ± 0.027	0.45 ± 0.053	50.88
RE_4	0.04 ± 0.009	0.02 ± 0.008	50.26
KE_4	0.53 ± 0.037	0.40 ± 0.056	50.10
KE_3	0.57 ± 0.019	0.46 ± 0.061	48.23
KE_2	0.48 ± 0.042	0.36 ± 0.059	45.54
KE_5	0.42 ± 0.046	0.29 ± 0.061	45.20
RE_2	0.03 ± 0.008	0.015 ± 0.006	43.64
RE_5	0.02 ± 0.006	0.008 ± 0.005	41.02
FD_4	3.89 ± 0.005	3.86 ± 0.021	40.10
KE_6	0.30 ± 0.061	0.17 ± 0.063	39.38
FD_2	3.88 ± 0.007	3.86 ± 0.017	38.96
FD_1	3.90 ± 0.003	3.88 ± 0.013	36.93
FD_5	3.87 ± 0.012	3.82 ± 0.034	35.73
FD_3	3.90 ± 0.003	3.87 ± 0.021	33.98
RE_6	0.01 ± 0.004	0.002 ± 0.002	32.24
KE_7	0.20 ± 0.043	0.13 ± 0.051	29.09
FD_7	3.76 ± 0.061	3.58 ± .0167	28.98
KE_8	0.10 ± 0.048	0.04 ± 0.035	25.33

mn: mean *std*: standard deviation.

2.5. Support vector machine classifier

In this work, support vector machine (SVM) classifier is employed to discriminate the two classes. SVM classifier [26] is a supervised machine learning algorithm which is widely used for classification. Supervised machine learning algorithms need labeled data in the training stage for mapping input-output pairs. In this work, a SVM classifier with polynomial kernel function of order 2 and 3 have been investigated. In the proposed approach, the ranked features obtained from each of R, G, and B channels are fed to three SVM classifiers separately for automated classification.

2.6. Decision level fusion

In order to effectively combine the information obtained from the three SVM classifiers, we explore decision level fusion scheme. Decision

Table 4
Classification performance based on various combinations of channels and order of polynomial kernel function.

Decision based on	Kernel parameter (polynomial order)	Accuracy (%)	Sensitivity (%)	Specificity (%)
R channel	2nd	98.36	96.78	99.52
R channel	3rd	98.60	97.97	99.05
G channel	2nd	98.95	98.83	99.05
G channel	3rd	98.98	98.20	99.52
B channel	2nd	98.81	98.99	98.70
B channel	3rd	98.74	98.33	99.05
Decision level fusion	2nd	99.16	98.99	99.29
Decision level fusion	**3rd**	**99.30**	**98.84**	**99.64**

Table 5
A comparative summary of the existing methods for automated glaucoma diagnosis.

Papers	Method	Number of images	Classifier	Performance parameters (%)
[4]	Fundus disk parameters	61	ANN	ac: 90.00 sn: 100 sp: 80.00
[34]	Retinal nerve fiber layer thickness	165	ANN	AROC: 0.932 sn: 83.54 sp: 93.02
[35]	Principal component analysis (PCA), fast Fourier transform (FFT) & spline interpolation	575	SVM	ac: 80.00 sn: 73.00 sp: 85.00
[2]	Higher order spectra (HOS) & texture features	60	RF	ac: 91.00 sn: NR sp: NR
[3]	Discrete wavelet transform (DWT) & texture features	60	SMO	ac: 93.00 sn: NR sp: NR
[36]	HOS & wavelet energy feature	60	SVM	ac: 95.00 sn: 93.33 sp: 96.67
[37]	HOS cumulant features	272	Naïve Bayesian	ac: 92.60 sn: 100 sp: 92.00
[38]	Gabor transfomation & texture and entropy features	510	SVM	ac: 93.10 sn: 89.75 sp: 96.20
[13]	Emperical wavelet transform (EWT) & correntropy	60	LS-SVM	ac: 98.33 sn: 100 sp: 96.67
[8]	Variational mode decomposition (VMD), entropy & fractal dimension	488	LS-SVM	ac: 95.19 sn: 93.62 sp: 96.71
[1]	Local configuration pattern (LCP) & texton	702	KNN	ac: 95.70 sn: 96.20 sp: 93.70
[39]	Non parametric spatial envelop energy spectrum	1000	SVM	ac: 97.00 sn: 97.80 sp: 95.80
[5]	Deep CNN	1426	CNN	ac: 98.13 sn: 98.00 sp: 98.30
Proposed method	**BPS & LBP**	**1426**	**SVM**	**ac: 99.30** **sn: 98.84** **sp: 99.64**

*NR = Not reported, ac = accuracy, sn = sensitivity, sp = specificity, AROC = Area under receiver operating characteristics.

level fusion combines the decisions made by multiple classifiers. In the proposed methodology, each of the three SVM classifiers generates a binary decision to indicate the normal and glaucoma class. In this fusion scheme, a query image is determined to be of a particular class, if the majority of classifiers generate decisions in favor of that class.

3. Results

The database used for performance evaluation in this work consists of 1426 retinal color fundus images, out of which 589 belong to the normal class and the rest belong to the glaucoma class. Images in this database have been collected at Kasturba Medical College, Manipal, India and we have obtained the ethical approval required for using the database in this work.

Individual R, G, and B channels are split into eight bit planes using BPS. The LBP is computed for each bit plane and three statistical features are extracted from each of the LBP images. The length of the feature vector generated by the above process is 24 for each of the R, G, and B channels. The extracted features from R, G, and B channels are listed in Tables 1–3, respectively with their corresponding *t* value. The 10-fold cross validation strategy [27] is employed to evaluate performance of the proposed methodology. The commonly used measures such as accuracy, sensitivity, and specificity [28] have been used for performance evaluation. Classification performance of our approach with different kernel parameters and decision methods are tabulated in Table 4. The results for individual channels with different polynomial orders are shown in Table 4. In addition, this table also shows results obtained using decision level fusion.

It can be observed from Table 4 that the minimum classification accuracy obtained is 98.36% for R channel. Similarly, the maximum classification accuracy obtained from individual channel is 98.98% for G channel. In addition, this table shows the performance obtained using decision level fusion scheme. The proposed approach achieves 99.30% classification accuracy with sensitivity and specificity of 98.83% and 99.64%, respectively using this fusion technique. It can be observed from Tables 1–3 that due to high *t* value of the features we obtain high classification accuracy. The plots of classification performance versus number of features with 2nd order and 3rd order polynomial kernel function are shown in Figs. 4 and 5, respectively.

4. Discussion

Previous methodologies have used gray texture analysis of images for the development of automated diagnosis systems for various diseases [1–3,13,29]. In this work, we have used bit level analysis for the development of automated system for glaucoma diagnosis. In the proposed methodology, BPS splits the individual R, G, and B channels of color fundus image into their corresponding bit planes. These bit planes contain bit level information of corresponding channels as shown in first and third rows of Fig. 3.

Generally, LBP is a texture operator that efficiently captures the changes in gray scale pixel variations. In this work, we have used LBP to capture the information that is present in bit planes. Second and fourth rows of Fig. 3 show the LBP images of the corresponding bit planes. Statistical features are used to capture the underlying texture variation from LBP images.

Kapur entropy, Renyi entropy, and fractal dimension effectively captures the information present in LBP images. In general, entropy is a measure of signal complexity or uncertainty. Renyi entropy and Kapur entropy based features have recently been investigated for different applications involving biomedical signal processing. Specifically, these entropies have been previously found to be effective for human seizure detection [30], identification of focal electroencephalogram (EEG) signals [31], and characterization of fatty liver disease [32]. The advantage of these entropies lies in their generality and flexibility due to the parameters involved, which enable several measurements of uncertainty. Fractal dimension is an indicator of the surface roughness and has previously been employed for thyroid lesion classification in ultrasound images [33]. The proven effectiveness of these features motivated us to explore them for fundus image based glaucoma diagnosis.

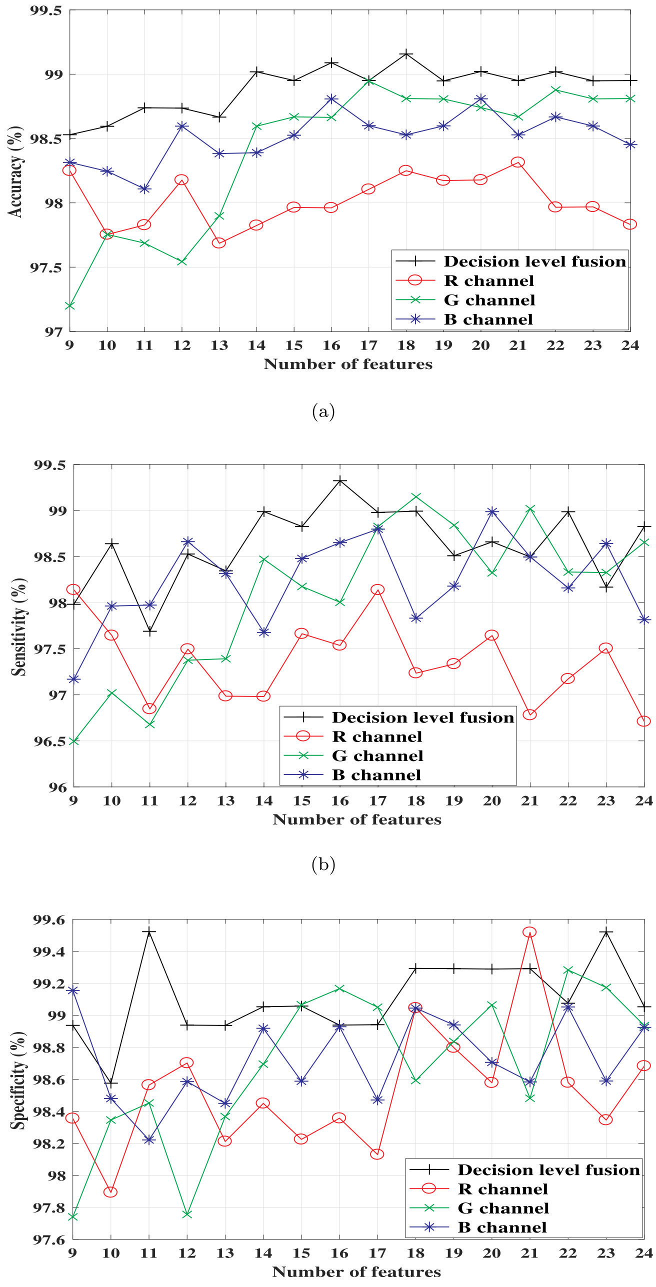

(a)

(b)

(c)

Fig. 4. Plot of classification performance versus number of features with 2nd order polynomial kernel.

It can be noted from Tables 1–3 that the mean value of features for normal cases are higher as compared to glaucoma cases. This is because, the normal image has more variations in terms of pixel intensities. In glaucoma case, the pixel intensity variations are less due to loss in retinal nerve fibers [13]. Also, the variability in entropy values of normal class is more as compared to the glaucoma as it has large optic disc (white region).

These results indicate that the features extracted from the individual channels alone are effective in discriminating the two classes. We have

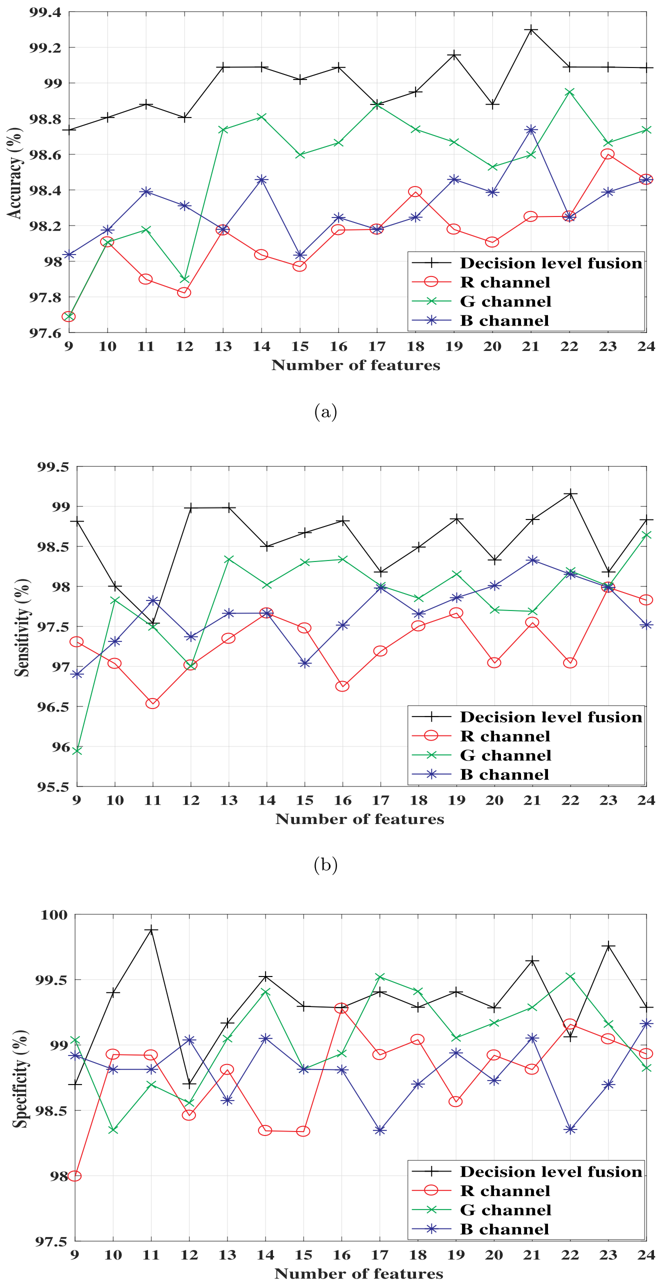

(a)

(b)

(c)

Fig. 5. Plot of classification performance versus number of features with 3^{rd} order polynomial kernel.

observed that the decision level fusion improves the overall performance of the proposed approach. Figs. 4 and 5 present the classification performance using individual channels and their decision level fusion. In summary, the proposed methodology provides the following advantages over the existing ones:

1. The proposed method achieved 98.64% sensitivity and 99.64% specificity using 21 number of features. Therefore, our method is effective in reducing the burden on the clinicians during the mass screening of patients.
2. The proposed method outperformed the existing methodologies for glaucoma diagnosis as it achieved the highest classification accuracy, when evaluated on a large dataset of fundus images.

The limitation of this study is that the proposed approach has not been evaluated on huge and diverse databases.

5. Conclusion

In this paper, we have presented a novel automated system for the diagnosis of glaucoma using bit-plane slicing and local binary patterns. In order to improve the overall performance, decision level based fusion technique is employed. The proposed methodology achieved a maximum classification accuracy of 99.30%. Also, high sensitivity and specificity values of the proposed method indicate that it can help in reducing burden on clinicians during mass screening. The proposed methodology outperformed the other existing glaucoma diagnosis methods. In future, we intend to extend the applicability of the proposed methodology for early stage diagnosis of glaucoma, age related macular degeneration, diabetic retinopathy and maculopathy. We also plan to develop state-of-the-art methodologies using deep learning techniques. The advantage of such methods is that one need not perform explicit feature extraction, statistical analysis, ranking and classification [5].

Acknowledgements

Not applicable.

References

[1] U.R. Acharya, S. Bhat, J.E. Koh, S.V. Bhandary, H. Adeli, A novel algorithm to detect glaucoma risk using texton and local configuration pattern features extracted from fundus images, Comput. Biol. Med. 88 (2017) 72–83.
[2] U.R. Acharya, S. Dua, X. Du, S.V. Sree, C.K. Chua, Automated diagnosis of glaucoma using texture and higher order spectra features, IEEE Trans. Inf. Technol. Biomed. 15 (3) (2011) 449–455.
[3] S. Dua, U.R. Acharya, P. Chowriappa, S.V. Sree, Wavelet based energy features for glaucomatous image classification, IEEE Trans. Inf. Technol. Biomed. 16 (1) (2012) 80–87.
[4] J. Nayak, U.R. Acharya, P.S. Bhat, N. Shetty, T.C. Lim, Automated diagnosis of glaucoma using digital fundus images, J. Med. Syst. 33 (5) (2009) 337–346.
[5] U. Raghavendra, H. Fujita, S.V. Bhandary, A. Gudigar, J.H. Tan, U.R. Acharya, Deep convolution neural network for accurate diagnosis of glaucoma using digital fundus images, Inf. Sci. 441 (2018) 41–49.
[6] Y. Hagiwara, J.E.W. Koh, J.H. Tan, S.V. Bhandary, A. Laude, E.J. Ciaccio, L. Tong, U.R. Acharya, Computer-aided diagnosis of glaucoma using fundus images: a review, Comput. Methods Progr. Biomed. 165 (2018) 1–12.
[7] K. Ganesan, R.J. Martis, U.R. Acharya, C.K. Chua, L.C. Min, E.Y.K. Ng, A. Laude, Computer-aided diabetic retinopathy detection using trace transforms on digital fundus images, Med. Biol. Eng. Comput. 52 (8) (2014) 663–672.
[8] S. Maheshwari, R.B. Pachori, V. Kanhangad, S.V. Bhandary, U.R. Acharya, Iterative variational mode decomposition based automated detection of glaucoma using fundus images, Comput. Biol. Med. 88 (2017) 142–149.
[9] U.R. Acharya, M.R.K. Mookiah, J.E. Koh, J.H. Tan, K. Noronha, S.V. Bhandary, A.K. Rao, Y. Hagiwara, C.K. Chua, A. Laude, Novel risk index for the identification of age-related macular degeneration using radon transform and {DWT} features, Comput. Biol. Med. 73 (2016) 131–140.
[10] J. Xu, O. Chutatape, P. Chew, Automated optic disk boundary detection by modified active contour model, IEEE (Inst. Electr. Electron. Eng.) Trans. Biomed. Eng. 54 (3) (2007) 473–482.
[11] G.D. Joshi, J. Sivaswamy, S.R. Krishnadas, Depth discontinuity-based cup segmentation from multiview color retinal images, IEEE (Inst. Electr. Electron. Eng.) Trans. Biomed. Eng. 59 (6) (2012) 1523–1531.
[12] A.D. Fleming, K.A. Goatman, S. Philip, J.A. Olson, P.F. Sharp, Automatic detection of retinal anatomy to assist diabetic retinopathy screening, Phys. Med. Biol. 52 (2) (2007) 331.
[13] S. Maheshwari, R.B. Pachori, U.R. Acharya, Automated diagnosis of glaucoma using empirical wavelet transform and correntropy features extracted from fundus images, IEEE Journal of Biomedical and Health Informatics 21 (3) (2017) 803–813.
[14] R.C. Gonzalez, R.E. Woods, Digital Image Processing, third ed., Prentice-Hall, Inc., Upper Saddle River, NJ, USA, 2006.
[15] K. Zuiderveld, Graphics Gems Iv, Academic Press Professional, Inc., San Diego, CA, USA, 1994, pp. 474–485 Ch. Contrast Limited Adaptive Histogram Equalization.
[16] T. Ojala, M. Pietikainen, T. Maenpaa, Multiresolution gray-scale and rotation invariant texture classification with local binary patterns, IEEE Trans. Pattern Anal. Mach. Intell. 24 (7) (2002) 971–987.
[17] M. Mookiah, U.R. Acharya, R.J. Martis, C.K. Chua, C. Lim, E. Ng, A. Laude, Evolutionary algorithm based classifier parameter tuning for automatic diabetic retinopathy grading: a hybrid feature extraction approach, Knowl. Base Syst. 39 (2013) 9–22.

[18] A. Pharwaha, B. Singh, Shannon and Non-shannon Measures of Entropy for Statistical Texture Feature Extraction in Digitized Mammograms Vol. 2 World Congress on Engineering and Computer Science, 2009.

[19] U.R. Acharya, M.R.K. Mookiah, J.E. Koh, J.H. Tan, S.V. Bhandary, A.K. Rao, H. Fujita, Y. Hagiwara, C.K. Chua, A. Laude, Automated screening system for retinal health using bi-dimensional empirical mode decomposition and integrated index, Comput. Biol. Med. 75 (2016) 54–62.

[20] U.R. Acharya, S.V. Sree, L. Saba, F. Molinari, S. Guerriero, J.S. Suri, Ovarian tumor characterization and classification using ultrasound—a new online paradigm, J. Digit. Imag. 26 (3) (2013) 544–553.

[21] M. Sharma, R.B. Pachori, U.R. Acharya, A new approach to characterize epileptic seizures using analytic time-frequency flexible wavelet transform and fractal dimension, Pattern Recogn. Lett. 94 (2017) 172–179.

[22] M.K. Biswas, T. Ghose, S. Guha, P.K. Biswas, Fractal dimension estimation for texture images: a parallel approach, Pattern Recogn. Lett. 19 (34) (1998) 309–313.

[23] M.H. Dunham, Data Mining: Introductory and Advanced Topics, Prentice Hall PTR, Upper Saddle River, NJ, USA, 2002.

[24] J.F. Box, Gosset Guinness, Fisher, and small samples, Stat. Sci. 2 (1) (1987) 45–52.

[25] U.R. Acharya, K.S. Vidya, D.N. Ghista, W.J.E. Lim, F. Molinari, M. Sankaranarayanan, Computer aided diagnosis of diabetic subjects by heart rate variability signals using discrete wavelet transform method, Knowl. Base Syst. 81 (2015) 56–64.

[26] C.J. Burges, A tutorial on support vector machines for pattern recognition, Data Min. Knowl. Discov. 2 (2) (1998) 121–167.

[27] R. Kohavi, A study of cross-validation and bootstrap for accuracy estimation and model selection, International Joint Conference on Artificial Intelligence, 14 1995, pp. 1137–1145.

[28] A.T. Azar, S.A. El-Said, Performance analysis of support vector machines classifiers in breast cancer mammography recognition, Neural Comput. Appl. 24 (5) (2014) 1163–1177.

[29] U.R. Acharya, S.V. Sree, M.M.R. Krishnan, F. Molinari, L. Saba, S.Y.S. Ho, A.T. Ahuja, S.C. Ho, A. Nicolaides, J.S. Suri, Atherosclerotic risk stratification strategy for carotid arteries using texture-based features, Ultrasound Med. Biol. 38 (6) (2012) 899–915.

[30] A. Feltane, G.F.B. Bartels, J. Gaitanis, Y. Boudria, W. Besio, Human seizure detection using quadratic rÃ©nyi entropy, 2013 6th International IEEE/EMBS Conference on Neural Engineering, NER), 2013, pp. 815–818.

[31] R. Sharma, R.B. Pachori, U.R. Acharya, Application of entropy measures on intrinsic mode functions for the automated identification of focal electroencephalogram signals, Entropy 17 (2) (2015) 669–691.

[32] U.R. Acharya, U. Raghavendra, H. Fujita, Y. Hagiwara, J.E. Koh, T.J. Hong, V.K. Sudarshan, A. Vijayananthan, C.H. Yeong, A. Gudigar, K.H. Ng, Automated characterization of fatty liver disease and cirrhosis using curvelet transform and entropy features extracted from ultrasound images, Comput. Biol. Med. 79 (2016) 250–258.

[33] U.R. Acharya, S.V. Sree, M.M.R. Krishnan, F. Molinari, R. Garberoglio, J.S. Suri, Non-invasive automated 3d thyroid lesion classification in ultrasound: a class of thyroscan systems, Ultrasonics 52 (4) (2012) 508–520.

[34] M.-L. Huang, H.-Y. Chen, W.-C. Huang, Y.-Y. Tsai, Linear discriminant analysis and artificial neural network for glaucoma diagnosis using scanning laser polarimetry–variable cornea compensation measurements in taiwan Chinese population, Graefe's Arch. Clin. Exp. Ophthalmol. 248 (3) (2010) 435–441.

[35] R. Bock, J. Meier, L.G. Nyúl, J. Hornegger, G. Michelson, Glaucoma risk index: automated glaucoma detection from color fundus images, Med. Image Anal. 14 (3) (2010) 471–481.

[36] M.R.K. Mookiah, U.R. Acharya, C.M. Lim, A. Petznick, J.S. Suri, Data mining technique for automated diagnosis of glaucoma using higher order spectra and wavelet energy features, Knowl. Base Syst. 33 (2012) 73–82.

[37] K.P. Noronha, U.R. Acharya, K.P. Nayak, R.J. Martis, S.V. Bhandary, Automated classification of glaucoma stages using higher order cumulant features, Biomed. Signal Process. Control 10 (2014) 174–183.

[38] U.R. Acharya, E. Ng, L.W.J. Eugene, K.P. Noronha, L.C. Min, K.P. Nayak, S.V. Bhandary, Decision support system for the glaucoma using Gabor transformation, Biomed. Signal Process. Control 15 (2015) 18–26.

[39] U. Raghavendra, S.V. Bhandary, A. Gudigar, U.R. Acharya, Novel expert system for glaucoma identification using non-parametric spatial envelope energy spectrum with fundus images, Biocybernetics and Biomedical Engineering 38 (1) (2018) 170–180.